

# Probe CP violation in $H \rightarrow \gamma Z$ through forward-backward asymmetry

Xuan Chen,<sup>1,2,\*</sup> Gang Li,<sup>1,†</sup> and Xia Wan<sup>3,‡</sup>

<sup>1</sup>*Institute of Theoretical Physics & State Key Laboratory of Nuclear Physics and Technology, Peking University, Beijing 100871, China*

<sup>2</sup>*Center for High Energy Physics, Peking University, Beijing 100871, China*

<sup>3</sup>*School of Physics & Information Technology, Shaanxi Normal University, Xi'an 710119, China*

(Dated: September 30, 2022)

## Abstract

We show that the forward-backward asymmetry ( $A_{FB}$ ) of the charged lepton in  $gg \rightarrow H \rightarrow \gamma Z \rightarrow \gamma \ell^- \ell^+$  process could be used to probe the CP violating  $H\gamma Z$  coupling when the interference of  $gg \rightarrow \gamma Z \rightarrow \gamma \ell^- \ell^+$  process is included. In the presence of CP violation in  $H\gamma Z$  coupling, the interference has a non-vanishing forward-backward asymmetry ( $A_{FB}$ ), which is also sensitive to the strong phase differences. The resonant and non-resonant strong phases together make  $A_{FB}$  change sign around Higgs mass  $M_H$ . We propose the integral over one-side mass region below (or above)  $M_H$  to get a larger  $A_{FB}$  in proton-proton collision.

---

\* xuan.chen@pku.edu.cn

† gangli@pku.edu.cn

‡ wanxia@snnu.edu.cn

## I. INTRODUCTION

To explain the observed matter-antimatter asymmetry in the universe, some CP-violation sources beyond Standard Model are needed [1, 2]. The newly discovered Higgs boson with mass around 125GeV may provide clues to search for CP violation. For example, the  $H \rightarrow ZZ \rightarrow 4l$  process is a golden channel to probe Higgs boson CP properties [3], since the momenta of four final state leptons could be used to directly construct a CP-odd triple product. The current measurement of  $H \rightarrow ZZ \rightarrow 4l$  [4] shows the CP odd/even mixture could be allowed around  $\sim 40\%$ . By contrast, the  $H \rightarrow \gamma Z$  or  $H \rightarrow \gamma\gamma$  processes are less considered when probing CP violation since these processes have only three or two final state momenta. However, after considering interference effects, several CP-violation observables could also be constructed. Some studies discussed the CP-violation observables in the  $H \rightarrow \gamma Z \rightarrow \gamma\ell^-\ell^+$  process: the forward-backward asymmetry ( $A_{FB}$ ) of the leptons in  $Z$  boson rest frame [5, 6], and the angle  $\phi$  between the  $Z$  production and decay planes [7].

At Large Hadron Collider (LHC), the Higgs boson is mainly produced by gluon fusion through a fermion loop. For  $gg \rightarrow H \rightarrow \gamma Z \rightarrow \gamma\ell^-\ell^+$  process,  $gg \rightarrow \gamma Z \rightarrow \gamma\ell^-\ell^+$  is an irreducible background process that could have interference effect. Ref. [7] studied such effect and found that the  $\phi$  angle between  $Z$  production and decay planes could be shifted by a weak phase from CP-violating  $H\gamma Z$  coupling, and thus is an CP-violation observable. Ref. [5] studied the  $A_{FB}$  through the interference with  $gg \rightarrow H \rightarrow \gamma\gamma^* \rightarrow \gamma\ell^-\ell^+$  process, and estimated that the integrated  $A_{FB}$  value is proportional to  $\frac{\Gamma_Z}{M_Z}$ . However, there is ambiguity about whether the CP-violation is from  $H \rightarrow \gamma Z$  or  $H \rightarrow \gamma\gamma$  vertices. If the couplings of both vertices have similar CP violation sources, thus have approximate weak phases, the  $A_{FB}$  value would be cancelled severely and become nearly zero. Ref. [6] studied the interferences not only between  $Z/\gamma$  propagators but also from  $H \rightarrow \gamma\ell^-\ell^+$  tree levels. It showed the  $A_{FB}$  distributions that are dependent on CP violation parameters in Yukawa couplings. In Ref. [8] the authors studied the CP violation in  $Ht\bar{t}$  coupling through  $e^+e^- \rightarrow H\gamma$  process, which is similar to the inverted process in our current work. However, the  $A_{FB}$  defined in Ref. [8] is different from the  $A_{FB}$  in our current work due to different kinematics.

The forward-backward asymmetry could be a CP violation observable because it could be considered as the asymmetry of producing CP conjugate final states  $F$  and  $\bar{F}$ . If the full

amplitude is the sum of two interfering amplitudes,  $M = |c_1|e^{i(\psi_1+\xi_1)} + |c_2|e^{i(\psi_2+\xi_2)}$ , where  $\psi_1, \psi_2$  are strong phases and  $\xi_1, \xi_2$  are weak phases, the asymmetry depends on the differences of both weak and strong phases:

$$A = \frac{\sigma(F) - \sigma(\bar{F})}{\sigma(F) + \sigma(\bar{F})} \propto |c_1||c_2| \sin(\psi_1 - \psi_2) \sin(\xi_1 - \xi_2) . \quad (1)$$

The CP violation could be probed only when both phase differences exist.

This paper is preformed in the following structure. In the first part, we introduce a general model with CP-violation phase factor and the helicity amplitudes involved for both signal and background processes. We also discuss the parity relations of those amplitudes. In the second part, a special frame with kinematic angles is introduced. We make a two-part factorization in such frame for the differential cross section and scrutinize the  $A_{FB}$  sources. In the third part, we setup numerical simulations using modified MCFM to estimate the  $A_{FB}$  values under different mass integral regions. In the last part, we summarize the results and discuss possible future work.

## II. HELICITY AMPLITUDES

### A. Effective operator and CP violation phase $\xi$

We use the following dimension-5 effective operators to describe the  $gg \rightarrow H \rightarrow \gamma Z$  process.

$$\mathcal{L}_h = \frac{c}{v} h F_{\mu\nu} Z^{\mu\nu} + \frac{\tilde{c}}{2v} h F_{\mu\nu} \tilde{Z}^{\mu\nu} + \frac{c_g}{v} h G_{\mu\nu}^a G^{a\mu\nu} . \quad (2)$$

Compare to Standard Model (SM), we add a CP-odd term to study the possible CP violation effects from  $H\gamma Z$  coupling, which may arise from CP violation in  $Hff$  Yukawa coupling,  $HVV$  coupling or other new physics. The Higgs boson couples to gluon via effective vertex where the top and bottom quarks are considered to be massive. The masses of the four light quarks are set to zero during our calculations. The source to bring CP violation in  $H\gamma Z$  coupling may also cause CP violation in  $Hgg$  coupling. However, it is beyond the scope of the current study.

Even though the  $c$  and  $\tilde{c}$  in Eq. (2) could be complex numbers and have different strong phases, here we make a simple assumption that both of them have equal strong phases. This is obviously true if CP violation happens in  $Ht\bar{t}$  or  $HVV$  vertex. In the following study we use the strong phase of  $H\gamma Z$  vertex in SM for both  $c$  and  $\tilde{c}$ .

We define a CP violation phase (weak phase)  $\xi$  through

$$\xi = \tan^{-1}(\tilde{c}/c), \quad (3)$$

when  $\xi = 0$ , it is the SM case; when  $\xi = \frac{\pi}{2}$ , only CP-odd  $H\gamma Z$  coupling exists. As  $\xi$  is the only weak phase, the CP observable is expected to be proportional to  $\sin \xi$ , which is also verified in our analytical calculations. Thus a non-zero  $A_{FB}$  means new physics, and new physics effects would be more obvious if  $A_{FB}$  reached its peak value at  $\xi = \frac{\pi}{2}$ .

### B. $gg \rightarrow H \rightarrow \gamma Z \rightarrow \gamma \ell^- \ell^+$ process

In this section, we firstly introduce the helicity amplitudes in spinor helicity formalism, then discuss their parity relations.

#### 1. Amplitudes in spinor helicity formalism

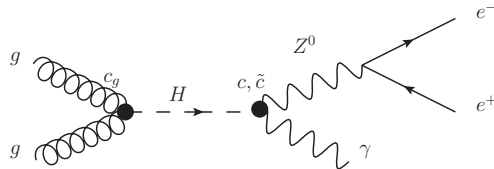


FIG. 1. The Feynman diagram of the process  $gg \rightarrow H \rightarrow \gamma Z \rightarrow \gamma \ell^- \ell^+$ . The  $c_g$  and  $c, \tilde{c}$  factors represent the  $Hgg$  and  $H\gamma Z$  effective couplings respectively.

Fig. 1 shows the Feynman diagram for the process of  $gg \rightarrow H \rightarrow \gamma Z \rightarrow \gamma \ell^- \ell^+$  as described by effective couplings in Eq. (2). The helicity amplitude is written into three parts,

$$\mathcal{A}_H(1_g^{h_1}, 2_g^{h_2}, 3_\gamma^{h_3}, 4_{\ell^-}^{h_4}, 5_{\ell^+}^{h_5}) = \mathcal{A}^{gg \rightarrow H}(1_g^{h_1}, 2_g^{h_2}) \times \frac{iP_H(s_{12})}{s_{12}} \times \mathcal{A}^{H \rightarrow \gamma Z \rightarrow \gamma \ell^- \ell^+}(3_\gamma^{h_3}, 4_{\ell^-}^{h_4}, 5_{\ell^+}^{h_5}), \quad (4)$$

where  $P_X(s) = \frac{s}{s - M_X^2 + iM_X\Gamma_X}$ ,  $s_{12} = (p_1 + p_2)^2$ .  $\mathcal{A}^{gg \rightarrow H}(1_g^{h_1}, 2_g^{h_2})$  is the helicity amplitude of gluon-gluon fusion to Higgs process, and  $h_1, h_2$  represents the helicities of outgoing gluons. When writing the helicity amplitudes, we adopt the conventions used in [9, 10]:

$$\begin{aligned} \langle ij \rangle &= \bar{u}_-(p_i)u_+(p_j), \quad [ij] = \bar{u}_+(p_i)u_-(p_j) \\ \langle ij \rangle [ij] &= 2p_i \cdot p_j, \quad s_{ij} = (p_i + p_j)^2, \end{aligned} \quad (5)$$

and we have

$$\begin{aligned}\mathcal{A}^{gg \rightarrow H}(1_g^+, 2_g^+) &= \frac{c_g}{v} [12]^2, \\ \mathcal{A}^{gg \rightarrow H}(1_g^-, 2_g^-) &= \frac{c_g}{v} \langle 12 \rangle^2.\end{aligned}\quad (6)$$

To keep the  $ggH$  coupling consistent with SM, we make

$$\frac{c_g}{v} = 1/2 \sum_f \frac{\delta^{C_1 C_2}}{2} \frac{i}{16\pi^2} g_s^2 4e \frac{m_f^2}{2M_W s_W} \frac{1}{M_H^2} (2 + M_H^2 (1 - \tau_H) C_0(m_f^2)), \quad (7)$$

where  $C_1, C_2 = 1, \dots, 8$  are  $SU(3)_c$  adjoint representation indices for the gluons,  $\tau_H = 4m_f^2/M_H^2$ , and the  $C_0(m^2)$  function is Passarino-Veltman three-point scalar functions [11].

The exact definition is given in Appendix A.

For all the other helicity amplitudes in this paper, we keep the convention that external legs are outgoing. After embedding the CP violation phase  $\xi$ , the helicity amplitudes of  $H \rightarrow \gamma Z \rightarrow \gamma \ell^- \ell^+$  are

$$\begin{aligned}\mathcal{A}^{H \rightarrow \gamma Z \rightarrow \gamma \ell^- \ell^+}(3_\gamma^+, 4_{\ell^-}^-, 5_{\ell^+}^+) &= 2 \frac{c}{v \cos \xi} e^{-i\xi} \times \frac{P_Z(s_{45})}{s_{45}} \frac{\langle 45 \rangle [35]^2}{\sqrt{2}} \times (el_e) \\ \mathcal{A}^{H \rightarrow \gamma Z \rightarrow \gamma \ell^- \ell^+}(3_\gamma^+, 4_{\ell^-}^+, 5_{\ell^+}^-) &= 2 \frac{c}{v \cos \xi} e^{-i\xi} \times \frac{P_Z(s_{45})}{s_{45}} \frac{\langle 45 \rangle [34]^2}{\sqrt{2}} \times (-er_e) \\ \mathcal{A}^{H \rightarrow \gamma Z \rightarrow \gamma \ell^- \ell^+}(3_\gamma^-, 4_{\ell^-}^-, 5_{\ell^+}^+) &= 2 \frac{c}{v \cos \xi} e^{i\xi} \times \frac{P_Z(s_{45})}{s_{45}} \frac{[45] \langle 34 \rangle^2}{\sqrt{2}} \times (el_e) \\ \mathcal{A}^{H \rightarrow \gamma Z \rightarrow \gamma \ell^- \ell^+}(3_\gamma^-, 4_{\ell^-}^+, 5_{\ell^+}^-) &= 2 \frac{c}{v \cos \xi} e^{i\xi} \times \frac{P_Z(s_{45})}{s_{45}} \frac{[45] \langle 35 \rangle^2}{\sqrt{2}} \sqrt{2} \times (-er_e),\end{aligned}\quad (8)$$

where  $s_{45} = (p_4 + p_5)^2$ ,  $l_e = v_f + a_f = \frac{-1+2s_W^2}{2s_W c_W}$  and  $r_e = v_f - a_f = \frac{2s_W^2}{2s_W c_W}$ .  $l_e$  and  $r_e$  are the left-hand and right-hand couplings of  $Z$  boson to leptons. We use the convention that  $\epsilon_\mu(p)/\epsilon_\mu^*(p)$  for outgoing/incoming photons.

The  $|\frac{c}{\cos \xi}|$  could be fixed by the total signal strength in experiment. Here we make a simple assumption that

$$\frac{c}{\cos \xi} = \sqrt{\mu_{SM}} c_{SM}, \quad (9)$$

where  $\mu_{SM}$  is the ratio of experimental signal strength to that SM predicts. In SM, the  $H\gamma Z$  coupling has no tree level contribution and the leading order contribution comes from the triangle loop diagrams induced by fermions and W boson. Thus we write

$$\frac{c_{SM}}{v} = 1/2(F_f^{HZ\gamma} + F_W^{HZ\gamma}) \quad (10)$$

with [12]

$$F_f^{HZ\gamma} = \sum_f N_c \frac{i}{16\pi^2} v_f Q_f 8e^3 \frac{m_f^2}{2M_W s_W} (C_0(m_f^2) + 4C_2(m_f^2)), \quad (11)$$

$$F_W^{HZ\gamma} = \frac{i}{16\pi^2} \frac{e^3}{M_W s_W} M_Z^2 \cot \theta_W \left[ \frac{2M_H^2}{M_W^2} (1-2c_W^2) C_2(M_W^2) + 4(1-6c_W^2) C_2(M_W^2) + 4(1-4c_W^2) C_0(M_W^2) \right]. \quad (12)$$

where  $v_f = \frac{I_f^3 - 2Q_f s_W^2}{2s_W c_W}$ ,  $I_f^3 = \pm \frac{1}{2}$ ,  $s_W = \sin \theta_W$ ,  $c_W = \cos \theta_W$  with  $\theta_W$  being the Weinberg angle, and the  $C_{0,2}(m^2)$  functions are Passarino-Veltman three-point scalar functions [11] as given in Appendix A.

## 2. Parity relation

The  $2 \rightarrow 3$  process could be factorized into a  $2 \rightarrow 2$  process times  $1 \rightarrow 2$  process,

$$\mathcal{A}_H(1_g^{h_1}, 2_g^{h_2}, 3_\gamma^{h_3}, 4_{\ell^-}^{h_4}, 5_{\ell^+}^{h_5}) = \mathcal{A}_H(1_g^{h_1}, 2_g^{h_2}, 3_\gamma^{h_3}, 45_Z^\kappa) \times \frac{iP_Z(s_{45})}{s_{45}} \times \mathcal{A}(45_Z^{-\kappa}, 4_{\ell^-}^{h_4}, 5_{\ell^+}^{h_5}), \quad (13)$$

where 45 represents the  $Z$  momentum with  $p_{45} = p_4 + p_5$ . We use  $-\kappa$  for the  $1 \rightarrow 2$  process because for both amplitudes  $\mathcal{A}_H(1_g^{h_1}, 2_g^{h_2}, 3_\gamma^{h_3}, 45_Z^\kappa)$  and  $\mathcal{A}(45_Z^{-\kappa}, 4_{\ell^-}^{h_4}, 5_{\ell^+}^{h_5})$  the external legs are all outgoing, thus for an incoming leg with helicity  $\kappa$  equivalent to an outgoing leg with flipped helicity  $-\kappa$ .

According to Eq.s (4), (6) and (8), the  $\xi$  dependent part could be extracted out as  $e^{-i\kappa\xi}$ , and the remaining part is the same as in the SM case. In  $2 \rightarrow 2$  process, we could write

$$\mathcal{A}_H(1_g^{h_1}, 2_g^{h_2}, 3_\gamma^{h_3}, 45_Z^\kappa) = \mathcal{A}_H^{SM}(1_g^{h_1}, 2_g^{h_2}, 3_\gamma^{h_3}, 45_Z^\kappa) \times e^{-i\kappa\xi}. \quad (14)$$

$\mathcal{A}_H^{SM}(1_g^{h_1}, 2_g^{h_2}, 3_\gamma^{h_3}, 45_Z^\kappa)$  is propagated by the Higgs boson and is non-zero only when  $h_1 = h_2$  and  $h_3 = \kappa$ . For the non-zero amplitudes, the parity relation is [7]

$$[\mathcal{A}_H^{SM \ 2 \rightarrow 2}]_{-h_3-\kappa}^{-h_1-h_2} = [\mathcal{A}_H^{SM \ 2 \rightarrow 2}]_{h_3\kappa}^{h_1h_2}. \quad (15)$$

The parity relation for  $\mathcal{A}_H(1_g^{h_1}, 2_g^{h_2}, 3_\gamma^{h_3}, 45_Z^\kappa)$  is

$$[\mathcal{A}_H^{2 \rightarrow 2}]_{-h_3-\kappa}^{-h_1-h_2} = [\mathcal{A}_H^{2 \rightarrow 2}]_{h_3\kappa}^{h_1h_2} \Big|_{\xi \leftrightarrow -\xi}. \quad (16)$$

$\xi$  changes sign under CP transformation and is a CP weak phase. This is understandable since  $\xi$  is connected to pseudoscalar coupling strength.

### C. $gg \rightarrow \gamma Z \rightarrow \gamma \ell^- \ell^+$ process

#### 1. Helicity amplitudes

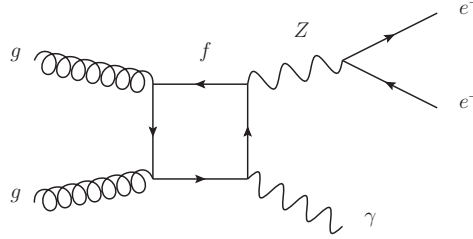


FIG. 2. The Feynman diagram of the process  $gg \rightarrow \gamma Z \rightarrow \gamma \ell^- \ell^+$ .

Fig. 2 shows the the Feynman diagram for the process of  $gg \rightarrow \gamma Z \rightarrow \gamma \ell^- \ell^+$ . The fermions in the loop include five light quarks. At the leading order of  $\alpha_s$  expansion, only box diagrams contribute to  $gg \rightarrow \gamma Z$  process [13]. The helicity amplitudes using the spinor helicity formalism are calculated in Ref. [13] and are coded in **MCFM** package. In the following numerical analysis, we use the helicity amplitudes in Eq.s (B.5)-(B.10) from Ref. [13]. We have checked the conventions carefully to make sure the interference with  $gg \rightarrow H \rightarrow \gamma Z \rightarrow \gamma \ell^- \ell^+$  amplitudes is correct.

#### 2. Parity relation

Under parity transformation the helicity amplitudes of  $gg \rightarrow \gamma Z$  behave like a high-spin d-matrix function [7]. The explicit expressions also support this viewpoint [14] and its parity relation is

$$[\mathcal{A}_{box}^{2 \rightarrow 2}]_{-h_3-\kappa}^{-h_1-h_2} = -(-1)^\kappa [\mathcal{A}_{box}^{2 \rightarrow 2}]_{h_3\kappa}^{h_1h_2}. \quad (17)$$

## III. KINEMATICS AND THE SOURCE OF $A_{FB}$

### A. The Angles

In the helicity amplitudes, we use  $p_i$  with  $i = 1 \cdots 5$  to represent momenta of the five external legs and write the process  $gg \rightarrow H \rightarrow \gamma Z \rightarrow \gamma \ell^- \ell^+$  as

$$g(p_1)g(p_2) \rightarrow H(p_{12}) \rightarrow \gamma(p_3)Z(p_{45}) \rightarrow \gamma(p_3)\ell^-(p_4)\ell^+(p_5), \quad (18)$$

where  $p_{12} = p_1 + p_2$ ,  $p_{45} = p_4 + p_5$ . Actually, the five momenta should fulfill the energy-momentum conservation criteria and we only need five variables to characterize the full kinematics. The independent variables are the two squared invariant masses  $s_{12}$  and  $s_{45}$ , and the three angles  $\theta$ ,  $\theta_1$  and  $\phi_1$ .

Fig. 3 illustrates the three angles.  $\theta$  is the angle between  $Z$  boson momentum direction

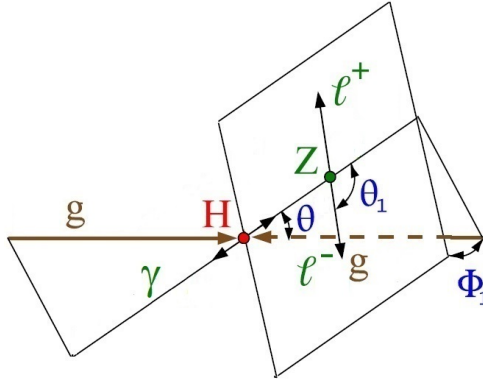


FIG. 3. The kinematic angles for  $gg \rightarrow H \rightarrow \gamma Z \rightarrow \gamma l^- l^+$  process.  $\theta$  is defined in  $H$  (or  $gg$ ) rest frame. It is the angle between  $Z$  boson momentum direction and  $Z$ -axis.  $\theta_1$  is the angle between  $l^-$  momentum in  $Z$  boson rest frame and  $Z$  boson production momentum which is obtained in  $H$  rest frame.  $\phi_1$  is the angle between  $Z$  boson production and decay planes.

and  $Z$ -axis in  $H$  (or  $gg$ ) rest frame.  $\theta \in [0, \pi]$ . For the background process,  $\theta$  is defined in the  $gg$  rest frame. In its expression we use  $-\vec{p}_3$  to represent  $Z$  boson momentum direction, that is

$$\theta = \cos^{-1} \left( -\frac{\vec{p}_3 \cdot \hat{n}_z}{|\vec{p}_3| |\hat{n}_z|} \right), \quad \hat{n}_z = (0, 0, 1). \quad (19)$$

$\theta_1$  is the angle between  $l^-$  momentum in  $Z$  boson rest frame and  $Z$  boson production momentum which is obtained in  $H$  rest frame.  $\theta_1 \in [0, \pi]$ . The expression for  $\theta_1$  is

$$\theta_1 = \cos^{-1} \left( -\frac{\vec{p}_3 \cdot \vec{p}_4}{|\vec{p}_3| |\vec{p}_4|} \right). \quad (20)$$

$\phi_1$  is the angle between the  $Z$  production and decay planes and  $\phi_1 \in [-\pi, \pi]$ . We define it in the  $H$  rest frame. It could also be defined in the  $Z$  rest frame since any boost along the  $Z$  direction won't change this angle. The expression for  $\phi_1$  is

$$\phi_1 = \frac{-\vec{p}_3 \cdot (\hat{n}_{prod} \times \hat{n}_{decay})}{|\vec{p}_3 \cdot (\hat{n}_{prod} \times \hat{n}_{decay})|} \times \cos^{-1}(\hat{n}_{prod} \cdot \hat{n}_{decay}), \quad (21)$$

with  $\hat{n}_{prod}$  and  $\hat{n}_{decay}$  being perpendicular to the corresponding planes, which are

$$\begin{aligned}\hat{n}_{prod} &= \frac{-\hat{n}_z \times \vec{p}_3}{|\hat{n}_z \times \vec{p}_3|}, \quad \hat{n}_z = (0, 0, 1) . \\ \hat{n}_{decay} &= \frac{\vec{p}_4 \times \vec{p}_5}{|\vec{p}_4 \times \vec{p}_5|} .\end{aligned}\quad (22)$$

## B. Cross Section Factorization

In this work we consider on-shell  $Z$  boson with narrow-width approximation for the  $Z$  boson propagator, that is  $\frac{P(s_{45})}{s_{45}} \rightarrow \pi \frac{1}{M_Z \Gamma_Z} \delta(s_{45} - M_Z^2)$ . The fully differential cross section is

$$\frac{d\hat{\sigma}(s_{12}, \theta; \theta_1, \phi_1)}{d(\cos \theta) d(\cos \theta_1) d\phi_1} = \frac{(s_{12} - M_Z^2)}{2^{11} \pi^3 s_{12}^2} \frac{|\mathcal{A}(s_{12}, \theta; \theta_1, \phi_1, \xi)|^2}{M_Z \Gamma_Z}, \quad (23)$$

where

$$\begin{aligned}|\mathcal{A}(s_{12}, \theta; \theta_1, \phi_1, \xi)|^2 &= \sum_{h_i} \left| \sum_{\kappa=+, 0, -} \mathcal{A}(1_g^{h_1}, 2_g^{h_2}, 3_\gamma^{h_3}, 45_Z^\kappa) \mathcal{A}(45_Z^{-\kappa}, 4_{\ell^-}^{h_4}, 5_{\ell^+}^{h_5}) \right|^2 \\ &= \sum_{h_i} \left| \sum_{\kappa=+, 0, -} [\mathcal{A}_H^{2 \rightarrow 2} + \mathcal{A}_{box}^{2 \rightarrow 2}]_{h_3 \kappa}^{h_1 h_2}(s_{12}, \theta, \xi) [\mathcal{A}^{1 \rightarrow 2}]_{h_4 h_5}^{-\kappa}(\theta_1, \phi_1) \right|^2 \\ &= \sum_{\kappa, \kappa'} [\tilde{\sigma}^{2 \rightarrow 2}]_{\kappa \kappa'}(s_{12}, \theta, \xi) [\tilde{\sigma}^{1 \rightarrow 2}]^{-\kappa - \kappa'}(\theta_1, \phi_1) \quad (24)\end{aligned}$$

with

$$\begin{aligned}[\tilde{\sigma}^{2 \rightarrow 2}]_{\kappa \kappa'}(s_{12}, \theta, \xi) &= \sum_{h_1, h_2, h_3} [\mathcal{A}_H^{2 \rightarrow 2} + \mathcal{A}_{box}^{2 \rightarrow 2}]_{h_3 \kappa}^{h_1 h_2}(s_{12}, \theta, \xi) [\mathcal{A}_H^{*2 \rightarrow 2} + \mathcal{A}_{box}^{*2 \rightarrow 2}]_{h_3 \kappa'}^{h_1 h_2}(s_{12}, \theta, \xi) , \\ [\tilde{\sigma}^{1 \rightarrow 2}]^{-\kappa - \kappa'}(\theta_1, \phi_1) &= \sum_{h_4, h_5} [\mathcal{A}^{1 \rightarrow 2}]_{h_4 h_5}^{-\kappa}(\theta_1, \phi_1) [\mathcal{A}^{*1 \rightarrow 2}]_{h_4 h_5}^{-\kappa'}(\theta_1, \phi_1) .\end{aligned}\quad (25)$$

The details of  $\tilde{\sigma}^{1 \rightarrow 2}$  and  $\tilde{\sigma}^{2 \rightarrow 2}$  are shown in the following sections and the source for  $A_{FB}$  is studied afterwards. More details involving the strong phase and mass integral region will be evaluated by the end of this chapter.

### 1. The $\tilde{\sigma}^{1 \rightarrow 2}$ contribution

In the  $Z$  rest frame, we choose

$$\begin{aligned}\epsilon^\mu(p_Z, \kappa = -) &= \frac{1}{\sqrt{2}}(0, 1, -i, 0) \\ \epsilon^\mu(p_Z, \kappa = +) &= \frac{1}{\sqrt{2}}(0, -1, -i, 0) \\ \epsilon^\mu(p_Z, \kappa = 0) &= (0, 0, 0, 1)\end{aligned}\quad (26)$$

Then the  $Z \rightarrow \ell^- \ell^+$  amplitudes are

$$\begin{aligned}
[\mathcal{A}^{1 \rightarrow 2}]_{+-}^+(\theta_1, \phi_1) &= \frac{1}{\sqrt{2}} M_Z r_e e^{i\phi_1} (1 + \cos \theta_1) \\
[\mathcal{A}^{1 \rightarrow 2}]_{-+}^+(\theta_1, \phi_1) &= -\frac{1}{\sqrt{2}} M_Z l_e e^{i\phi_1} (1 - \cos \theta_1) \\
[\mathcal{A}^{1 \rightarrow 2}]_{+-}^-(\theta_1, \phi_1) &= \frac{1}{\sqrt{2}} M_Z r_e e^{-i\phi_1} (1 - \cos \theta_1) \\
[\mathcal{A}^{1 \rightarrow 2}]_{-+}^-(\theta_1, \phi_1) &= -\frac{1}{\sqrt{2}} M_Z l_e e^{-i\phi_1} (1 + \cos \theta_1) \\
[\mathcal{A}^{1 \rightarrow 2}]_{+-}^0(\theta_1, \phi_1) &= M_Z r_e \sin \theta_1 \\
[\mathcal{A}^{1 \rightarrow 2}]_{-+}^0(\theta_1, \phi_1) &= M_Z l_e \sin \theta_1
\end{aligned} \tag{27}$$

Thus the  $[\tilde{\sigma}^{1 \rightarrow 2}]^{\kappa \kappa'}$  could be written in the matrix form as

$$\begin{aligned}
&\begin{pmatrix} [\tilde{\sigma}^{1 \rightarrow 2}]^{--} & [\tilde{\sigma}^{1 \rightarrow 2}]^{-0} & [\tilde{\sigma}^{1 \rightarrow 2}]^{-+} \\ [\tilde{\sigma}^{1 \rightarrow 2}]^{0-} & [\tilde{\sigma}^{1 \rightarrow 2}]^{00} & [\tilde{\sigma}^{1 \rightarrow 2}]^{0+} \\ [\tilde{\sigma}^{1 \rightarrow 2}]^{+-} & [\tilde{\sigma}^{1 \rightarrow 2}]^{+0} & [\tilde{\sigma}^{1 \rightarrow 2}]^{++} \end{pmatrix} \\
&= \frac{M_Z^2}{2} \begin{pmatrix} (r_e^2 + l_e^2)(1 + \cos^2 \theta_1) & (r_e^2 - l_e^2)\sqrt{2} \sin \theta_1 e^{-i\phi_1} & (r_e^2 + l_e^2)(1 - \cos^2 \theta_1)e^{-i2\phi_1} \\ (r_e^2 - l_e^2)\sqrt{2} \sin \theta_1 e^{i\phi_1} & (r_e^2 + l_e^2)2 \sin^2 \theta_1 & (r_e^2 - l_e^2)\sqrt{2} \sin \theta_1 e^{-i\phi_1} \\ (r_e^2 + l_e^2)(1 - \cos^2 \theta_1)e^{i2\phi_1} & (r_e^2 - l_e^2)\sqrt{2} \sin \theta_1 e^{i\phi_1} & (r_e^2 + l_e^2)(1 + \cos^2 \theta_1) \end{pmatrix} \\
&+ \frac{M_Z^2}{2} \cos \theta_1 \begin{pmatrix} -2(r_e^2 - l_e^2) & -(r_e^2 + l_e^2)\sqrt{2} \sin \theta_1 e^{-i\phi_1} & 0 \\ -(r_e^2 + l_e^2)\sqrt{2} \sin \theta_1 e^{i\phi_1} & 0 & (r_e^2 + l_e^2)\sqrt{2} \sin \theta_1 e^{-i\phi_1} \\ 0 & (r_e^2 + l_e^2)\sqrt{2} \sin \theta_1 e^{i\phi_1} & 2(r_e^2 - l_e^2) \end{pmatrix}
\end{aligned} \tag{28}$$

We split up the  $[\tilde{\sigma}^{1 \rightarrow 2}]^{\kappa \kappa'}$  matrix into  $\cos \theta$  symmetric and asymmetric parts. Notice that when  $\kappa \neq \kappa'$ , the  $[\tilde{\sigma}^{1 \rightarrow 2}]^{\kappa \kappa'}$  terms depend on  $\phi_1$  and have zero contribution to the cross section after  $\phi_1$  integral (from  $-\pi$  to  $\pi$ ). That is

$$\int_{-\pi}^{\pi} d\phi_1 [\tilde{\sigma}^{1 \rightarrow 2}]^{\kappa \kappa'}(\theta_1, \phi_1) = 0, \quad \kappa \neq \kappa' \tag{29}$$

Only  $\kappa = \kappa'$  terms could contribute after the  $\phi_1$  integral. Thus for  $A_{FB}$  value we only need to focus on the  $\kappa = \kappa'$  case.

## 2. The $\tilde{\sigma}^{2 \rightarrow 2}$ contribution

By factorizing out the  $\xi$  dependence in  $\tilde{\sigma}^{2 \rightarrow 2}$ , one would have

$$\begin{aligned} [\tilde{\sigma}^{2 \rightarrow 2}]_{\kappa\kappa'}(s_{12}, \theta, \xi) &= [\tilde{\sigma}_{H,H}^{2 \rightarrow 2}]_{\kappa\kappa'}(s_{12}, \theta) + [\tilde{\sigma}_{box,box}^{2 \rightarrow 2}]_{\kappa\kappa'}(s_{12}, \theta) \\ &+ [\tilde{\sigma}_{H,box}^{2 \rightarrow 2}]_{\kappa\kappa'}(s_{12}, \theta)e^{-i\kappa\xi} + [\tilde{\sigma}_{box,H}^{2 \rightarrow 2}]_{\kappa\kappa'}(s_{12}, \theta)e^{i\kappa'\xi}, \end{aligned} \quad (30)$$

where  $[\tilde{\sigma}_{H,H}^{2 \rightarrow 2}]$  represents the contribution from  $gg \rightarrow H \rightarrow \gamma Z$  process,  $[\tilde{\sigma}_{box,box}^{2 \rightarrow 2}]$  represents the contribution from  $gg \rightarrow \gamma Z$  process, and  $[\tilde{\sigma}_{H,box}^{2 \rightarrow 2}]$  represents their interference.

According to Eqs. (16), (17) and the definition of complex conjugate, we have the following identities:

$$[\tilde{\sigma}_{H/box,H/box}^{2 \rightarrow 2}]_{+,+} = [\tilde{\sigma}_{H/box,H/box}^{2 \rightarrow 2}]_{-,-} \quad (31)$$

$$[\tilde{\sigma}_{box,H}^{2 \rightarrow 2}]_{\kappa\kappa'} = [\tilde{\sigma}_{H,box}^{2 \rightarrow 2}]_{\kappa\kappa'}^*. \quad (32)$$

Applying Eqs. (31) and (32) to (30), one would have

$$[\tilde{\sigma}^{2 \rightarrow 2}]_{++} - [\tilde{\sigma}^{2 \rightarrow 2}]_{--} = 4 \operatorname{Im}[\tilde{\sigma}_{H,box}^{2 \rightarrow 2}]_{++} \sin \xi \quad (33)$$

$$[\tilde{\sigma}^{2 \rightarrow 2}]_{++} + [\tilde{\sigma}^{2 \rightarrow 2}]_{--} = 2[\tilde{\sigma}_{H,H}^{2 \rightarrow 2}]_{++} + 2[\tilde{\sigma}_{box,box}^{2 \rightarrow 2}]_{++} + 4 \operatorname{Re}[\tilde{\sigma}_{H,box}^{2 \rightarrow 2}]_{++} \cos \xi \quad (34)$$

$$[\tilde{\sigma}^{2 \rightarrow 2}]_{00} = [\tilde{\sigma}_{box,box}^{2 \rightarrow 2}]_{00}. \quad (35)$$

## C. The source of $A_{FB}$

Firstly, we get  $A_{FB}(s_{12})$  in gluon-gluon fusion from the above differential cross sections. Secondly, we connect it to the  $A_{FB}$  in proton-proton collision through the convolution with parton distribution function. Finally, we show the non-resonant strong phases make  $A_{FB}$  change sign around the resonant peak and propose an mass integral region asymmetric around the resonant peak to enhance  $A_{FB}$ .

### 1. $A_{FB}(s_{12})$ in gluon-gluon fusion

Combining Eqs. (23), (24), (28) and (35), we could get

$$\frac{d\hat{\sigma}(s_{12}, \theta; \theta_1, \phi_1)}{d(\cos \theta_1)} = \frac{(s_{12} - M_Z^2)}{2^{11}\pi^3 s_{12}^2 M_Z \Gamma_Z} \left\{ (r_e^2 + l_e^2) \int_{-1}^1 d\cos \theta \int_{-\pi}^{\pi} d\phi_1 ([\tilde{\sigma}^{2 \rightarrow 2}]_{++} + [\tilde{\sigma}^{2 \rightarrow 2}]_{--})(1 + \cos^2 \theta_1) \right. \\ + 2(r_e^2 + l_e^2) \int_{-1}^1 d\cos \theta \int_{-\pi}^{\pi} d\phi_1 [\tilde{\sigma}^{2 \rightarrow 2}]_{00} \sin^2 \theta_1 \\ \left. + 2(l_e^2 - r_e^2) \int_{-1}^1 d\cos \theta \int_{-\pi}^{\pi} d\phi_1 ([\tilde{\sigma}^{2 \rightarrow 2}]_{++} - [\tilde{\sigma}^{2 \rightarrow 2}]_{--}) \cos \theta_1 \right\}.$$

The forward-backward asymmetry in gluon-gluon fusion is

$$A_{FB}(s_{12}) = \frac{N_F(s_{12}) - N_B(s_{12})}{N_F(s_{12}) + N_B(s_{12})} \quad (36)$$

$$= \frac{(\int_0^1 - \int_{-1}^0) d\cos \theta_1 \int_{-1}^1 d\cos \theta \int_{-\pi}^{\pi} d\phi_1 \frac{d\hat{\sigma}(s_{12}, \theta; \theta_1, \phi_1)}{d(\cos \theta) d(\cos \theta_1) d\phi_1}}{(\int_{-1}^1) d\cos \theta_1 \int_{-1}^1 d\cos \theta \int_{-\pi}^{\pi} d\phi_1 \frac{d\hat{\sigma}(s_{12}, \theta; \theta_1, \phi_1)}{d(\cos \theta) d(\cos \theta_1) d\phi_1}} \quad (37)$$

$$= \frac{3(l_e^2 - r_e^2) \int_{-1}^1 d\cos \theta \text{Im}[\tilde{\sigma}_{H,box}^{2 \rightarrow 2}]_{++} \sin \xi}{(r_e^2 + l_e^2) \int_{-1}^1 d\cos \theta (2[\tilde{\sigma}_{H,H}^{2 \rightarrow 2}]_{++} + 2[\tilde{\sigma}_{box,box}^{2 \rightarrow 2}]_{++} + 4 \text{Re}[\tilde{\sigma}_{H,box}^{2 \rightarrow 2}]_{++} \cos \xi + [\tilde{\sigma}^{2 \rightarrow 2}]_{00})} \quad (38)$$

The denominator of  $A_{FB}(s_{12})$  includes signal and background cross sections as well as the interference part which is proportional to  $\cos \xi$ . The numerator is proportional to  $\sin \xi$ . In the SM case, where  $\xi = 0$ , no  $A_{FB}(s_{12})$  could be observed. When  $\xi = \frac{\pi}{2}$ ,  $A_{FB}(s_{12})$  is non-zero and reaches its potential largest value. The details depend on both the imaginary and real parts of  $[\tilde{\sigma}_{H,box}^{2 \rightarrow 2}]_{++}$ .

### 2. $A_{FB}$ in proton-proton collision

The proton-proton differential cross section is

$$\frac{d\sigma_{pp \rightarrow \gamma Z}}{d(\sqrt{s_{12}}) d(\cos \theta_1)} = 2\sqrt{s_{12}} G(s_{12}) \frac{d\hat{\sigma}(s_{12}, \theta_1)}{d(\cos \theta_1)}, \quad (39)$$

where  $\sqrt{s_{12}} = M_{\gamma Z}$ ,  $s$  being the total hadronic c.m. energy and

$$G(s_{12}) = \int_{s_{12}/s}^1 \frac{dx}{sx} [g(x) g(s_{12}/(sx))]. \quad (40)$$

The forward-backward asymmetry in proton-proton collision is

$$A_{FB} = \frac{N_F - N_B}{N_F + N_B} \quad (41)$$

$$= \frac{(\int_0^1 - \int_{-1}^0) d\cos \theta_1 \int_I d\sqrt{s_{12}} \frac{d\sigma_{pp \rightarrow \gamma Z}}{d(\sqrt{s_{12}}) d(\cos \theta_1)}}{(\int_{-1}^1) d\cos \theta_1 \int_I d\sqrt{s_{12}} \frac{d\sigma_{pp \rightarrow \gamma Z}}{d(\sqrt{s_{12}}) d(\cos \theta_1)}}, \quad (42)$$

where  $\int_I$  represents an mass region to be integrated. The integral kernel in numerator is proportional to  $\text{Im}[\tilde{\sigma}_{H,box}^{2 \rightarrow 2}]_{++}$ , so we further study its dependence on  $\sqrt{s_{12}}$  to search for the suitable mass integral region.

### 3. Strong phase and mass integral region

The strong phase  $\psi_1$  in  $gg \rightarrow H \rightarrow \gamma Z$  process has three sources: Higgs propagator,  $Hgg$  vertex and  $H\gamma Z$  vertex. With its finite width, Higgs propagator provides a strong phase that is small when far away from resonance, but increase rapidly to  $\frac{\pi}{2}$  at  $M_H$ . The  $Hgg$  and  $H\gamma Z$  vertices get small strong phases ( $\sim \text{arctan}(0.01)$  or less) from bottom loop diagrams since  $M_H > 2M_b$ . The strong phase  $\psi_2$  in  $gg \rightarrow \gamma Z$  process could be introduced by light quarks (with five active flavours), which may also be suppressed by light quarks' small mass. With the assumption of zero-mass limit, the same-helicity  $g^\pm g^\pm \rightarrow f\bar{f}$  process is absent.

If one extracts the strong phase  $\psi'_1 = \tan^{-1} \frac{-M_H \Gamma_H}{s - M_H^2}$  from Higgs resonance, the other strong phases (non-resonant strong phases) depend more smoothly on  $\sqrt{s_{12}}$ . For this reason, we write

$$\begin{aligned} \text{Im}[\tilde{\sigma}^{2 \rightarrow 2}]_{++} \propto & -\text{Im}(\mathcal{A}^{gg \rightarrow H} \mathcal{A}^{H \rightarrow \gamma Z} \mathcal{A}_{box}^{*gg \rightarrow \gamma Z}) \frac{s_{12} - M_H^2}{(s_{12} - M_H^2)^2 + M_H^2 \Gamma_H^2} \\ & + \text{Re}(\mathcal{A}^{gg \rightarrow H} \mathcal{A}^{H \rightarrow \gamma Z} \mathcal{A}_{box}^{*gg \rightarrow \gamma Z}) \frac{M_H \Gamma_H}{(s_{12} - M_H^2)^2 + M_H^2 \Gamma_H^2} \end{aligned} \quad (43)$$

and define a new strong phase by  $\psi = \psi_1 - \psi'_1 - \psi_2$  which is

$$\psi = \tan^{-1} \frac{\text{Im}(\mathcal{A}^{gg \rightarrow H} \mathcal{A}^{H \rightarrow \gamma Z} \mathcal{A}_{box}^{*gg \rightarrow \gamma Z})}{\text{Re}(\mathcal{A}^{gg \rightarrow H} \mathcal{A}^{H \rightarrow \gamma Z} \mathcal{A}_{box}^{*gg \rightarrow \gamma Z})}. \quad (44)$$

From above expressions of  $\psi$  and  $\psi'_1$ , one can rewrite Eq. (43) and get  $\text{Im}[\tilde{\sigma}^{2 \rightarrow 2}]_{++} \propto \sin(\psi_1 - \psi_2)$ , which is consistent with Eq. (1).

Fig. 4 shows  $\text{Im}[\tilde{\sigma}^{2 \rightarrow 2}]_{++}$  versus  $\sqrt{s_{12}}$  for different  $\psi$  values. The  $M_H$  and  $\Gamma_H$  are set as 126GeV and 4.3MeV respectively. If  $\psi = 0$ , it is the black line that is symmetric around  $M_H$ , which is positive through the whole mass region; if  $\psi$  is non-zero,  $\text{Im}[\tilde{\sigma}^{2 \rightarrow 2}]_{++}$  changes sign around resonant peak. For  $\psi = \frac{\pi}{2}$  it changes sign at resonant peak; for  $\psi = \frac{\pi}{4}$  it changes sign when  $\sqrt{s_{12}} \approx M_H + \frac{\Gamma_H}{2}$ . The asymmetric line has a long flat tail when  $\sqrt{s_{12}}$  is a few GeV far away from the resonant peak, but the symmetric line drops more rapidly. After integrated by half region blow  $M_H$ , for example [124, 126]GeV, the asymmetric line gets 4

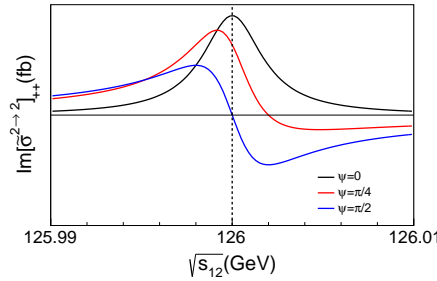


FIG. 4.  $\text{Im}[\tilde{\sigma}^{2 \rightarrow 2}]_{++}$  versus  $\sqrt{s_{12}}$  for different  $\psi$  values.  $M_H = 126 \text{ GeV}$ , and  $\Gamma_H = 4.3 \text{ MeV}$ .

times larger of the integrated value than the symmetric one. For  $\psi = \frac{\pi}{4}$ , integral over  $[124, 126] \text{ GeV}$  is about 3 times of integral over  $[124, 128] \text{ GeV}$ .

The integral kernel of  $A_{FB}$  also changes sign as  $\text{Im}[\tilde{\sigma}^{2 \rightarrow 2}]_{++}$ . So choosing a mass integral region in which  $\text{Im}[\tilde{\sigma}^{2 \rightarrow 2}]_{++}$  always keeps same sign is key factor to enhance  $A_{FB}$ . When resonant width is very small, a mass region one-side below or above resonant peak could fulfill this criterion and supply a relatively large  $A_{FB}$ . Thus in the following simulation we make a comparison for  $A_{FB}$  values from one-side mass integral region and symmetric mass integral region.

#### IV. SIMULATION

The simulations to quantify interference effects and the value of  $A_{FB}$  is preformed using **MCFM** package. We adopt the amplitudes for  $gg \rightarrow \gamma Z \rightarrow \gamma \ell^- \ell^+$  process from **MCFM** and add amplitudes for  $gg \rightarrow H \rightarrow \gamma Z \rightarrow \gamma \ell^- \ell^+$  as described in previous sections. The simulations are generated for a proton-proton collider with  $\sqrt{s} = 14 \text{ TeV}$ . The final state photon is required to have  $p_T^\gamma > 20 \text{ GeV}$  and  $\eta^\gamma < 2.5$ . The  $\ell^- \ell^+$  invariant mass is set to be in  $Z$  boson mass region, that is  $M_{\ell^- \ell^+} \in [66, 116] \text{ GeV}$ .

Fig. 5 left panel shows the fiducial differential cross section for  $gg \rightarrow \gamma Z \rightarrow \gamma \ell^- \ell^+$  process including the  $gg \rightarrow H \rightarrow \gamma Z \rightarrow \gamma \ell^- \ell^+$  process and their interference part. The peak at  $M_H = 126 \text{ GeV}$  is the Higgs resonance and the width of the peak is about  $4.3 \text{ MeV}$ . In the high mass region, the cross section decreases slowly as  $M_{\gamma Z}$  increases. The blue and red histograms represent  $\xi = 0$  and  $\xi = \frac{\pi}{2}$  cases respectively. They have small difference at the resonant region caused by interference effects. Fig. 5 right panel shows only the interference contribution, which is calculated by  $|M_H + M_{bg}|^2 - |M_H|^2 - |M_{bg}|^2$ . For both cases when

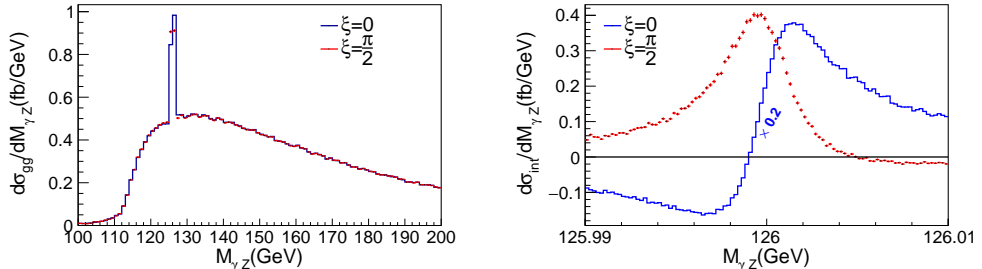


FIG. 5. *Left panel:* The  $M_{\gamma Z}$  differential cross section for  $\xi = 0$  (blue histogram) and  $\xi = \frac{\pi}{2}$  (red histogram with error bars) cases. *Right panel:* The  $M_{\gamma Z}$  differential cross section integrated over  $\cos \theta_1$  from 0 to 1 of only the interference part ( $|M_H + M_{bg}|^2 - |M_H|^2 - |M_{bg}|^2$ ). The blue histogram is scaled by  $\times 0.2$ .

$\xi = 0$  or  $\frac{\pi}{2}$ , we integrate only half region of  $\cos \theta_1$  (from 0 to 1) to keep the contribution from  $\cos \theta_1$ -odd terms. This treatment is based on the fact that when  $\xi = \frac{\pi}{2}$  the  $\cos \theta_1$  distribution of the interference part is asymmetric (see Fig. 6). When  $\xi = 0$ , the interference contribution is proportional to  $\text{Re}[\tilde{\sigma}_{H,box}^{2 \rightarrow 2}]_{++}$  (the blue histogram), which also consists of large asymmetric contribution. We multiply it by 0.2 for better comparison. When  $\xi = \frac{\pi}{2}$ , the interference contribution is proportional to  $\text{Im}[\tilde{\sigma}_{H,box}^{2 \rightarrow 2}]_{++}$  (the red histogram with error bars). From the shape of the red histogram, the peak position is shifted to left by about 1MeV, and the cross section reaches to zero at about  $M_{\gamma Z} = 126.004\text{GeV}$ . It corresponds to  $\tan \psi \sim 0.5$ . The integral over only half region below  $M_H$  could increase the numerator of  $A_{FB}$  while decrease the denominator by half. In the following analysis, we preform the integration in the lower half region of  $M_{\gamma Z}$  to study the enhanced  $A_{FB}$  effect.

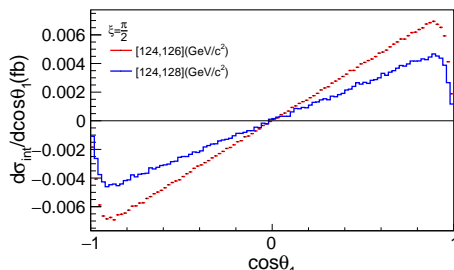


FIG. 6.  $d\sigma_{int}/d \cos \theta_1$  versus  $\cos \theta_1$  when  $\xi = \frac{\pi}{2}$  for  $[124, 126]\text{GeV}$  integral region (red histogram with error bars) and  $[124, 128]\text{GeV}$  integral region (blue histogram).

Fig. 6 shows the differential cross section of  $\cos \theta_1$  (with  $\xi = \frac{\pi}{2}$ ). The slope is equal to

the numerator value of  $A_{FB}$ . When integrating over [124, 126]GeV, the slope is about 0.008. By contrast, the slope is about 0.005 when integrating over [124, 128]GeV. Together with the total cross section,  $A_{FB}$  values under different integral regions are shown in Table I. It could reach about 0.6% inside [124, 126]GeV region, but 2 times smaller for the symmetric [124, 128]GeV region.

TABLE I.  $A_{FB}$  values under different integral mass regions.

Integral mass region(GeV)	$A_{FB}$ numerator (fb)	$A_{FB}$ denominator (fb)	$A_{FB}$
[124, 126]	0.008	1.4	$\sim 0.57\%$
[124, 128]	0.005	2.8	$\sim 0.18\%$

The significance is estimated as the following: after the fiducial cuts of  $M_{\ell-\ell^+} \in [66, 116]$ GeV,  $M_{\gamma Z} \in [124, 126]$ GeV,  $p_T^\gamma > 20$ GeV and  $\eta^\gamma < 2.5$ , for  $\xi = \frac{\pi}{2}$ , the total cross section with interference effect of  $gg \rightarrow \gamma Z \rightarrow \gamma \ell^- \ell^+$  and  $gg \rightarrow H \rightarrow \gamma Z \rightarrow \gamma \ell^- \ell^+$  is  $\sigma_{gg} = 1.4$ fb, the cross section for background  $q\bar{q} \rightarrow \gamma Z$  process is  $\sigma_{q\bar{q}} = 40.8$ fb. According to the definition of the significance

$$\frac{S}{\sqrt{B}} = \frac{A_{FB}\sigma_{gg}L}{\sqrt{\sigma_{q\bar{q}}L}} \sim \frac{A_{FB}}{0.08} \sqrt{\frac{L}{3000\text{fb}^{-1}}}, \quad (45)$$

to reach a significance  $\sim 1$ , the  $A_{FB}$  effect from the interference contribution should be one order larger. After LHC reaching the  $3000\text{fb}^{-1}$  luminosity, such  $A_{FB}$  effect would still be difficult to distinguish. However, it leaves possibility for new physics which could introduce both large CP-violation phases and interference effect.

## V. CONCLUSION AND DISCUSSION

In this work we construct a model with general CP violation phase  $\xi$  from  $H\gamma Z$  coupling. By calculating the interference effect between  $gg \rightarrow H \rightarrow \gamma Z \rightarrow \gamma \ell^- \ell^+$  and  $gg \rightarrow \gamma Z \rightarrow \gamma \ell^- \ell^+$  processes, we confirm that the forward-backward asymmetry  $A_{FB}$  of charged leptons in the  $Z$  rest frame is a  $H\gamma Z$  CP-violation observable, and is proportional to  $\sin \xi$ . We analyze the impact of several non-zero strong phases which is also a key factor to determine the value of  $A_{FB}$ . After checking the lineshape of integral kernel, we propose to do integral of  $M_{\gamma Z}$  over half of the resonant mass region to get a larger  $A_{FB}$ . After detailed simulations

using modified MCFM, we estimate the  $A_{FB}$  could reach about 0.6%. After considering the huge amount of  $q\bar{q}$  initial process, the significance is relatively small and hard to be observed at the high-luminosity phase of LHC. More detailed studies involving non-zero strong phases and mass regions of  $M_{\gamma Z}$  could be preformed under similar frameworks. The analysis also reveals that new physics with large CP-violation phases may not be easily ruled out when searching for forward-backward asymmetry at the LHC.

## ACKNOWLEDGMENTS

X.W. thanks Youkai Wang for valuable discussions about the cross section factorization and  $A_{FB}$  definition. We thank Yandong Liu and Chih-Hao Fu for helpful discussions. X.W. is supported by the National Science Foundation of China under Grant No. 11405102. The work was also supported in part by the National Science Foundation of China under Grant No. 11135003, No. 11635001 and No. 11375014.

## Appendix A: Definition of Passarino-Veltman three-point scalar functions

For the Higgs production and decay processes, the Passarino-Veltman three-point scalar functions  $C_0(m^2)$  and  $C_2(m^2)$  have simple forms in terms of  $\tau_Z = 4m^2/M_Z^2$  and  $\tau_H = 4m^2/M_H^2$ :

$$4m^2C_0(m^2) = -\frac{2\tau_Z\tau_H}{\tau_Z - \tau_H} [f(\tau_Z) - f(\tau_H)] , \quad (A1)$$

$$4m^2C_2(m^2) = \frac{\tau_Z\tau_H}{2(\tau_Z - \tau_H)} + \frac{\tau_Z\tau_H^2}{2(\tau_Z - \tau_H)^2} \left( \tau_Z [f(\tau_Z) - f(\tau_H)] + 2 [g(\tau_Z) - g(\tau_H)] \right) \quad (A2)$$

with the functions  $f$  and  $g$  are defined by

$$f(\tau) = \begin{cases} \arcsin^2 \sqrt{1/\tau} & \tau \geq 1 \\ -\frac{1}{4} \left[ \log \frac{1+\sqrt{1-\tau}}{1-\sqrt{1-\tau}} - i\pi \right]^2 & \tau < 1 \end{cases} \quad (A3)$$

$$g(\tau) = \begin{cases} \sqrt{\tau-1} \arcsin \sqrt{1/\tau} & \tau \geq 1 \\ \frac{1}{2} \sqrt{1-\tau} \left[ \log \frac{1+\sqrt{1-\tau}}{1-\sqrt{1-\tau}} - i\pi \right] & \tau < 1 \end{cases} \quad (A4)$$

---

[1] M. B. Gavela, P. Hernandez, J. Orloff, and O. Pene, Mod. Phys. Lett. **A9**, 795 (1994), arXiv:hep-ph/9312215.

- [2] A. D. Sakharov, *Pisma Zh. Eksp. Teor. Fiz.* **5**, 32 (1967), [*Usp. Fiz. Nauk* **161**, 61 (1991)].
- [3] Y. Chen, R. Harnik, and R. Vega-Morales, *Phys. Rev. Lett.* **113**, 191801 (2014), arXiv:1404.1336.
- [4] CMS, V. Khachatryan *et al.*, *Phys. Rev.* **D92**, 012004 (2015), arXiv:1411.3441.
- [5] Y. Chen, A. Falkowski, I. Low, and R. Vega-Morales, *Phys. Rev.* **D90**, 113006 (2014), arXiv:1405.6723.
- [6] A. Yu. Korchin and V. A. Kovalchuk, *Eur. Phys. J.* **C74**, 3141 (2014), arXiv:1408.0342.
- [7] M. Farina, Y. Grossman, and D. J. Robinson, *Phys. Rev.* **D92**, 073007 (2015), arXiv:1503.06470.
- [8] G. Li, H.-R. Wang, and S.-h. Zhu, *Phys. Rev.* **D93**, 055038 (2016), arXiv:1506.06453.
- [9] L. J. Dixon, Calculating scattering amplitudes efficiently, in *QCD and beyond. Proceedings, Theoretical Advanced Study Institute in Elementary Particle Physics, TASI-95, Boulder, USA, June 4-30, 1995*, pp. 539–584, 1996, arXiv:hep-ph/9601359.
- [10] J. M. Campbell, R. K. Ellis, and C. Williams, *JHEP* **04**, 060 (2014), arXiv:1311.3589.
- [11] G. Passarino and M. J. G. Veltman, *Nucl. Phys.* **B160**, 151 (1979).
- [12] A. Djouadi, V. Driesen, W. Hollik, and A. Kraft, *Eur. Phys. J.* **C1**, 163 (1998), arXiv:hep-ph/9701342.
- [13] J. M. Campbell, R. K. Ellis, and C. Williams, *JHEP* **07**, 018 (2011), arXiv:1105.0020.
- [14] L. Ametller, E. Gava, N. Paver, and D. Treleani, *Phys. Rev.* **D32**, 1699 (1985).